Inorganic Chemistry

Article

pubs.acs.org/IC

Dihydrogen Bonding in Complex $(PP_3)RuH(\eta^1\text{-}BH_4)$ Featuring Two Proton-Accepting Hydride Sites: Experimental and Theoretical Studies

Natalia V. Belkova,[†] Ekaterina V. Bakhmutova-Albert,[†] Evgenii I. Gutsul,[†] Vladimir I. Bakhmutov,[†] Igor E. Golub,[†] Oleg A. Filippov,[†] Lina M. Epstein,[†] Maurizio Peruzzini,*[,‡] Andrea Rossin,[‡] Fabrizio Zanobini,[‡] and Elena S. Shubina*[,†]

[†]A.N. Nesmeyanov Institute of Organoelement Compounds, Russian Academy of Sciences, 28 Vavilov Street, 119991 Moscow, Russia

[‡]Istituto di Chimica dei Composti Organometallici, Consiglio Nazionale delle Ricerche (ICCOM-CNR), via Madonna del Piano 10, 50019 Sesto Fiorentino (Florence), Italy

Supporting Information

ABSTRACT: Combining variable-temperature infrared and NMR spectroscopic studies with quantum-chemical calculations (density functional theory (DFT) and natural bond orbital) allowed us to address the problem of competition between MH (M = transition metal) and BH hydrogens as proton-accepting sites in dihydrogen bond (DHB) and to unravel the mechanism of proton transfer to complex $(PP_3)RuH(\eta^1\text{-}BH_4)$ (**1**, PP_3 = κ^4-$P(CH_2CH_2PPh_2)_3$). Interaction of complex **1** with CH_3OH, fluorinated alcohols of variable acid strength [CH_2FCH_2OH, CF_3CH_2OH, $(CF_3)_2CHOH$ (HFIP), $(CF_3)_3COH$], and CF_3COOH leads to the medium-strength DHB complexes involving BH bonds (3−5 kcal/mol), whereas DHB complexes with RuH were not observed experimentally. The two proton-transfer pathways were considered in DFT/M06 calculations. The first one goes via more favorable bifurcate complexes to BH_{term} and high activation barriers (38.2 and 28.4 kcal/mol in case of HFIP) and leads directly to the thermodynamic product $[(PP_3)RuH_{eq}(H_2)]^+[OR]^-$. The second pathway starts from the less-favorable complex with RuH ligand but shows a lower activation barrier (23.5 kcal/mol for HFIP) and eventually leads to the final product via the isomerization of intermediate $[(PP_3)RuH_{ax}(H_2)]^+[OR]^-$. The B−$H_{br}$ bond breaking is the common key step of all pathways investigated.

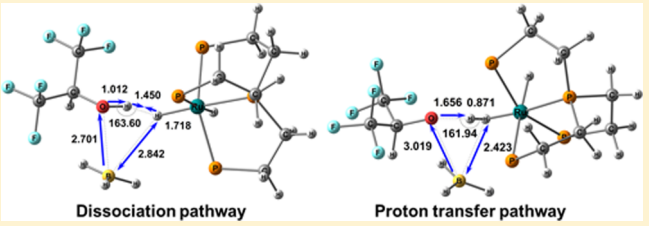

INTRODUCTION

Coordination compounds containing the simplest hydroborate anion BH_4^- as a ligand possess many valuable properties. Tetrahydroborate complexes of transition metal ions are indeed used as selective reducing agents,[1−9] starting compounds in the synthesis of complex and organometallic derivatives,[10] precursors for the production of borides,[11] hydrides,[12] and other inorganic materials, and as effective catalysts of hydrogenation,[13−15] isomerization,[16] oligomerization,[17] polymerization,[18−21] etc. In addition, these complexes exhibit unusual structural and dynamic properties, such as the ability to form M−H−B (M = transition metal) multicenter bonds, and display exceptionally low barriers to the intramolecular exchange of bridging and terminal hydrogen atoms in the tetrahydroborate ligand.[22−25]

It is well recognized that both transition metal hydrides and boron hydrides can form the unusual hydrogen bonds with proton donors where the hydride ligand acts as proton acceptor.[26−28] These hydride−proton interactions, widely referred to as dihydrogen bonds (DHBs), play an important role in proton-transfer reactions.[29,30] Moreover, the formation of these nonclassical H-bonds has been recently established to be a general property of hydride ligands. For example, DHBs of metal tetrahydroborates[31] and main group hydrides (EH) with proton donors (HX), that is, the EH···HX interaction, have been found in solution[32−34] and in solid state.[35,36] The strength of different DHB complexes has been determined. Thus, anionic tetrahydroborates and tetrahydrogallates as well as transition metal hydrides give the medium-strength DHB adducts with different proton donors (4.0−7.6 kcal/mol),[29,33] while neutral boron hydrides, like $(EtO)_3PBH_3$ and Et_3NBH_3, form weak DHBs (2.5−3.3 kcal/mol).[32] The nonclassical proton-accepting site (BH) can successfully compete with the classical ones (e.g., CN). The mutual influence of the two proton-accepting sites has been shown by some of us on both the polyhedral boron hydride ($[B_{12}H_{11}SCN]^{2-}$) and the cyanoborohydride ($[BH_3CN]^-$).[34,37]

Recently we reported on the experimental and theoretical study of the interaction between different proton donors and

Received: October 17, 2013
Published: December 26, 2013

   dx.doi.org/10.1021/ic4026206 | Inorg. Chem. 2014, 53, 1080−1090

the BH_4^- ligand coordinated to a copper (I) center in the complex $(Ph_3P)_2Cu(\eta^2\text{-}BH_4)$.[31] The diversity of DHB complexes was shown by density functional theory (DFT) calculations, which revealed the competition between the bridging and terminal BH groups as proton-accepting sites. Bifurcate complexes involving both bridging and terminal hydride hydrogen atoms become thermodynamically preferred for strong proton donors, in agreement with the experiment. The mechanism of the proton transfer and dimerization intermediated by the bifurcate DHB complexes was evaluated.

Recently, ruthenium and iron hydrido tetrahydroborate pincer complexes $MH(BH_4)(PNP)$ (PNP = (2,6-bis-(dialkylphosphinomethyl)pyridine) have been reported to efficiently catalyze the base-free hydrogenation of organic carbonyl compounds as well as the dehydrogenation of alcohols.[14,15] NMR studies on the iron complexes have suggested that the tetrahydroborate ligand dissociates prior to the ketone reduction.[15] Interestingly, the ^1H NMR of $FeH(CO)(\eta^1\text{-}BH_4)(PNP)$ in CD_3OH has shown the presence of species with a weaker association of the coordinated tetrahydroborate ligand,[15] but the possible formation of DHB was not taken into account to explain this finding. Moreover, the mechanism of the BH_4^- dissociation and generation of catalytically active species has not been discussed yet. To better address the problem of M−H bond activation (M = transition metal or boron) in the presence of alcohols, we decided to study the interaction of the complex $(PP_3)RuH(\eta^1\text{-}BH_4)$ (**1**)[38] (PP_3 = $\kappa^4\text{-}P(CH_2CH_2PPh_2)_3$, Chart 1) with proton donors.

Chart 1

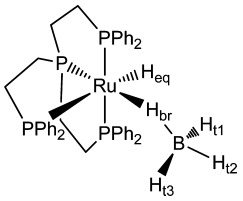

According to Peruzzini et al.,[38] protonation of complex **1** by strong acids yielded the cationic dihydrogen complex $[(PP_3)\text{-}RuH(\eta^2\text{-}H_2)]^+$, a nonclassical trihydride which could be also prepared by the straightforward protonation of the corresponding dihydride $(PP_3)RuH_2$.[39]

The aims of this paper were to study the competition between the two proton-accepting sites (RuH and BH) and to elucidate the role of different DHB complexes in the proton-transfer mechanism. The interaction between complex **1** and a variety of proton donors with different acid strength [MeOH, fluorinated alcohols R^FOH = CH_2FCH_2OH (MFE), CF_3CH_2OH (TFE), $(CF_3)_2CHOH$ (HFIP), $(CF_3)_3COH$ (PFTB), and CF_3COOH (TFA)] was studied by variable-temperature (VT) infrared (IR) and NMR spectroscopy in combination with DFT/M06 calculations.

EXPERIMENTAL SECTION

General Considerations. The complex $(PP_3)RuH(\eta^1\text{-}BH_4)$ (**1**) was synthesized according to the published procedure.[38] All manipulations were performed under a dry argon atmosphere using standard Schlenk techniques. Dichloromethane was purified by standard procedures using CaH_2 before being freshly distilled under argon prior to use. Fluorinated alcohols were provided by P and M (Moscow, Russia) and used without further purification. Other reagents were obtained from Sigma Aldrich.

Variable-Temperature IR Measurements. IR spectra were recorded on Specord M82 and Infralum FTIR-81 (Lumex) spectrometers in CH_2Cl_2 solutions using 0.04−0.12 cm CaF_2 cells. Low-temperature IR studies were carried out in the 190−300 K temperature range using a home-modified cryostat (Carl Zeiss Jena). Cryostat modification allows transfer of the reagents (premixed at either low or room temperature) under an inert atmosphere directly into the cell. For measurements in the ν_{OH} region, the acid concentrations were 10^{-2}−10^{-3} M to avoid self-association, whereas the concentration of complex **1** was taken in 10-fold excess. For measurements in the ν_{BH} range, the equimolar ratio or 10-fold excess acids were used. The spectra in this region are reported after the subtraction of the overtones of PP_3 ligand vibrations (ν_{CH} and ν_{CC} of phenyl rings).[39]

^1H T_1 Relaxation Time Measurements. ^1H NMR experiments (200 MHz) were performed with a Bruker WP-200 spectrometer, where tetramethylsilane was used as an internal standard. The spin−lattice relaxation time measurements were carried out by the standard inversion−recovery method. Radio frequency pulses were carefully calibrated at different temperatures. The exponential inversion−recovery curves were treated with standard software of the spectrometer to show errors of <10% in the T_1 calculations. The proton−hydride interactions were investigated in cold (190 K) CD_2Cl_2 solutions in 5 mm NMR tubes, and all the NMR experiments were run starting at low temperature with the precooled NMR probe head.

Computational Details. Full geometry optimizations were carried out with the *Gaussian09*[40] package using density functional theory (DFT) with the M06 functional.[41] A simplified model system was exploited for the simulation of the proton-transfer reaction, where the phenyl substituents on PP_3 were replaced with methyl groups, to achieve a shorter computational time. Effective core potentials (ECPs) and their associated SDD basis set supported with *f*-function polarization were used to represent the innermost electrons of the ruthenium atom.[42,43] The basis sets used were 6-311G(d) for the phosphorus atoms,[44] 6-311++G(d,p) for the BH_4^- fragment, ruthenium bound hydrogen, and the alcohol OH group.[45,46] The 6-31G basis set[45] was used for all other atoms. Frequency calculations were performed for all optimized complexes in the gas phase, and the vibrational frequencies are reported without the use of scaling factors. The nature of all the stationary points on the potential energy surfaces was confirmed by a vibrational analysis.[47] Transition state (TS) structures showed only one negative eigenvalue in their diagonalized force constant matrices, and their associated eigenvectors were confirmed to correspond to the motion along the reaction coordinate. Intrinsic reaction coordinate (IRC)[48] calculations were carried out in both directions starting from the located transition states to prove connection between reactants and products.

Natural atomic charges and Wiberg bond indices[49] (WBIs) were calculated using the natural-bond orbital (NBO) analysis[50] implemented in *Gaussian09*. Topological analysis of the electron-density distribution function $\rho(r)$ was performed using the *AIMALL*[51] program package based on the wave function obtained by the M06 calculations. The energies of H···H interactions were calculated using the correlation between the binding energy ($E_{H\cdots H}$) and the value of the density-functional potential energy $V(r)$ in the corresponding critical point (3, −1): $E_{H\cdots H} = 0.5 \times V(r)$.[52,53] Hydrogen bond ellipticity $\varepsilon_{H\cdots H}$ was defined as $\varepsilon = (\lambda_1/\lambda_2 - 1)$, where λ_1 and λ_2 are the negative eigenvalues of the Hessian of the electron density at the bond critical point ordered such that $\lambda_1 < \lambda_2 < 0$.[54−56]

RESULTS AND DISCUSSION

IR Study of DHB Formation with Alcohols. Upon room-temperature addition of an excess of complex $(PP_3)RuH(\eta^1\text{-}BH_4)$ (**1**) to the R^FOH solution in CH_2Cl_2 (R^FOH = FCH_2CH_2OH (MFE), CF_3CH_2OH (TFE), $(CF_3)_2CHOH$ (HFIP)), the IR spectra in the ν_{OH} region show new low-frequency shifted broad bands of ν_{OH}^{bond}, evidencing the H-bond formation (Figure 1).

dx.doi.org/10.1021/ic4026206 | Inorg. Chem. 2014, 53, 1080−1090

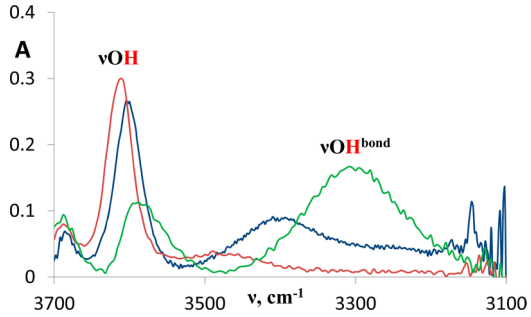

Figure 1. IR spectra in the ν_{OH} region of alcohols: (a) TFE (0.030 M): complex **1** (0.060 M), blue line; (b) MFE (0.020 M): complex **1** (0.051 M), red line; (c) HFIP (0.020 M): complex **1** (0.051 M), green line. CH_2Cl_2, 298 K, l = 1.2 mm.

The frequency shift ($\Delta\nu_{OH} = \nu_{OH}^{bond} - \nu_{OH}^{free}$) increases with the increase of the proton-donating ability (P_i)[29] of R^FOH as in all hydrogen-bonded systems (see Table 1). The frequency shift values are typical of hydrogen bonding; from these figures it is possible to determine the formation enthalpies and the basicity factors E_j, see below.

Table 1. Spectroscopic Characteristics of DHB Complexes between 1 and OH Acids

OH	P_i	ν_{OH}^{free}, cm^{-1}	ν_{OH}^{bond}, cm^{-1}	$\Delta\nu_{OH}$, cm^{-1}	$-\Delta H^\circ_{exp}$, kcal/mol
MFE	0.78	3612	3467	−145	3.0
TFE	0.89	3602	3400	−202	3.9
		3604	3392	−212	4.1
HFIP	1.05	3584	3300	−284	5.1

However, for hydrides possessing two competing sites (nonclassical and classical), the two ν_{OH}^{bond} bands assigned to DHB (OH···HB) and to classical hydrogen bond (OH···NCS or OH···NC) can overlap.[12] The observation of only one bonded band for complex **1**·R^FOH (Figure 1) does not allow us to say whether it belongs to one of the two possible DHBs (BH···HO or RuH···HO) or to both. To solve this problem the IR spectra in the range of the ligand stretching vibrations (ν_{RuH} and ν_{BH}) were studied, analyzing the changes caused by R^FOH addition, as reported in our previously published work.[32] The following rule for the H-bonding site determination was used:[29] the band of the proton-accepting group shifts to lower frequency (negative $\Delta\nu$), while all other bands shift to higher frequencies (positive $\Delta\nu$), where $\Delta\nu = \nu^{bond} - \nu^{free}$.

The IR spectra of free hydride **1** (Figure 2) exhibit broad bands due to the terminal BH groups vibrations ($\nu_{BH_{term}}$) at 2362 and 2292 cm^{-1} (CH_2Cl_2). Two other bands, at 2046 and 1902 cm^{-1}, belong to $\nu_{BH_{br}}$ and ν_{RuH}.[38] In the presence of HFIP in the 200−230 K temperature range, the low-frequency shifts of $\nu_{BH_{term}}$ ($\Delta\nu_{BH_{term}}{}^{as}$ by −8 cm^{-1} and $\nu_{BH_{term}}{}^{s}$ by −17 cm^{-1}) and the high-frequency shifts of the $\nu_{BH_{br}}$ band (by +17 cm^{-1}) and the ν_{RuH} band (by +6 cm^{-1}) were revealed (Figures 1 and 6). These wavenumber variations prove the formation of the DHB with the terminal BH group as the proton-accepting site (eq 1). Therefore, both RuH and bridging BH hydride ligands remain nonbonded. A similar spectroscopic behavior was observed for complex **1** in the presence of TFE and PFTB.

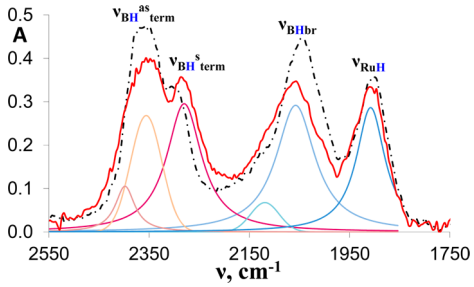

Figure 2. IR spectra in the ν_{MH} region: complex **1** (0.021 M, black dash-dot line); complex **1** (0.06 M) in the presence of HFIP (0.03 M, red solid line), CH_2Cl_2, l = 0.12 mm at 200 K. Bands deconvolution is shown by thin colored lines.

$$(PP_3)RuH(\eta^1\text{-}BH_4) + ROH \leftrightarrows (PP_3)RuH(\eta^1\text{-}BH_3H)\cdots HOR \quad (1)$$

DHB Strength. The hydrogen bond formation enthalpy ($-\Delta H^\circ$, Table 1) was determined by using the Iogansen's empirical correlation (eq 2).[57−60]

$$-\Delta H^\circ = \frac{18\Delta\nu_{XH}}{720 + \Delta\nu_{XH}} \quad (2)$$

The basicity factor (eq 3)[27,29,56] characterizes the proton-accepting ability in hydrogen bond independent of proton donor and solvent.

$$E_j = \frac{\Delta H^\circ}{\Delta H_{11} P_i} \quad (3)$$

The value of the basicity factor determined for complex **1**, E_j = 0.98 ± 0.04, is less than that of the tetrahydroborate anion (E_j = 1.25).[61] This can be explained by the decrease of the electron density on the hydride ligands due to the coordination of BH_4^- to the ruthenium center. Nonetheless, the proton-accepting ability of the coordinated BH_4^- is higher than that of the neutral boron trihydrides and polyhedral anionic boranes.[32,34,62,63]

NMR Study of Interaction with Alcohols. The hydride region of the ^1H NMR spectrum of complex **1** (0.031 M) shows the RuH resonance (doublet of triplets) at −8.993 ppm in CD_2Cl_2 at 220 K. The BH_4^- group of the same complex exhibits a very broadened line (−1.53 ppm) due to an exchange between the terminal and bridging BH atoms.[38] This exchange is stopped on the NMR time scale at 190 K: the unique bridging BH resonance (−10.33 ppm) is well observed in the spectrum, while the other three terminal BH atoms give a very broadened line at 1.35 ppm. The RuH chemical shift of complex **1** is essentially independent from the temperature in the 190−240 K range (−8.986 and −8.993 ppm, respectively). T_1 relaxation measurements gave for complex **1** the $T_{1\,min}$(RuH) value of 0.178 s (200 K, 200 MHz). Unfortunately, it was difficult to characterize accurately the T_1(BH) temperature dependence for the BH_4^- resonance because it is strongly broadened due to the above-mentioned exchange. Nevertheless the averaged BH_4^- resonance of complex **1** showed a T_1 time of 0.21 and 0.13 s at 220 and 200 K, respectively. In addition, the bridging BH resonance of complex **1** appearing in the spectrum at 190 K (see above) exhibits the T_1 time of 0.16 s. As mentioned above, the minimum of T_1 for the RuH line is reached at 200 K. Hence the value of 0.13 s

dx.doi.org/10.1021/ic4026206 | Inorg. Chem. 2014, 53, 1080−1090

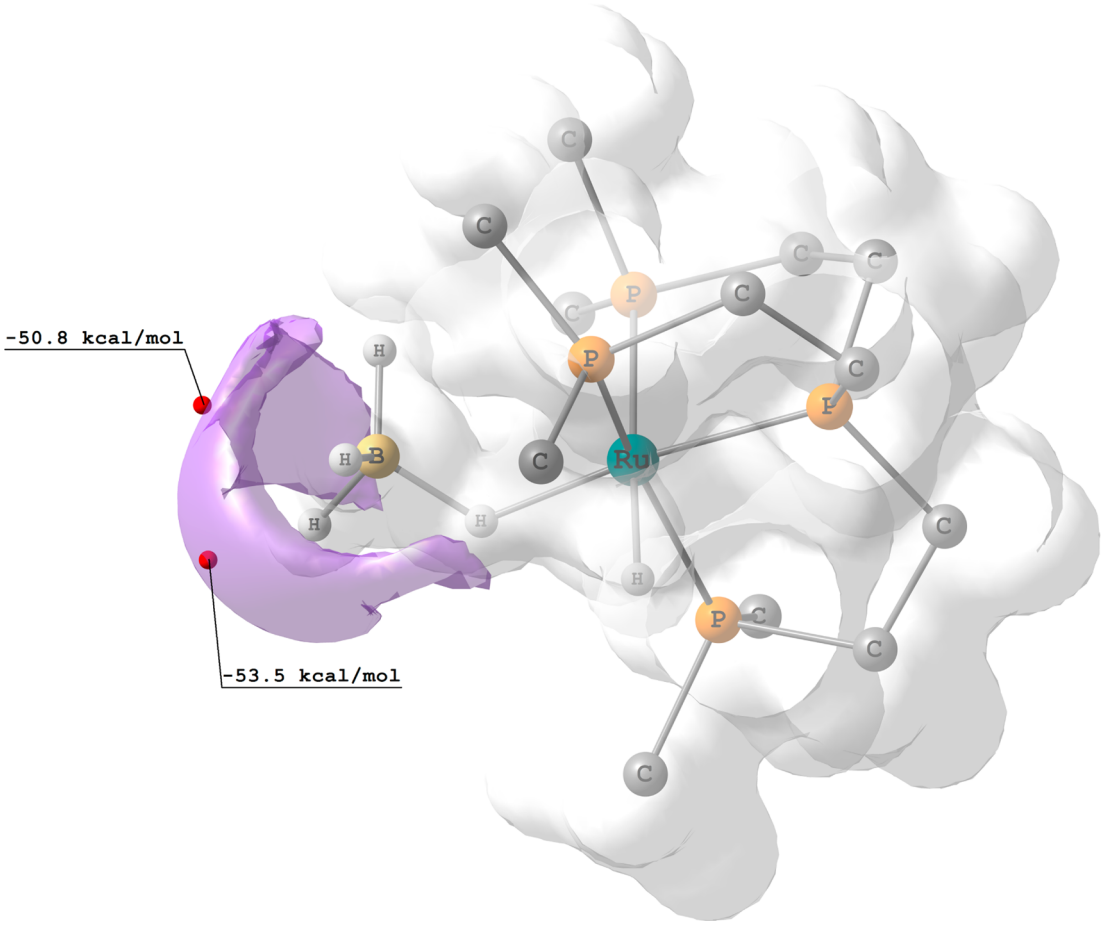

Figure 3. Molecular electrostatic potential of complex **2** as isosurface at 0.0833 au. Extremes of electrostatic potential V_{min} indicated by red dots. H-atoms of PP_3-ligand are omitted for clarity.

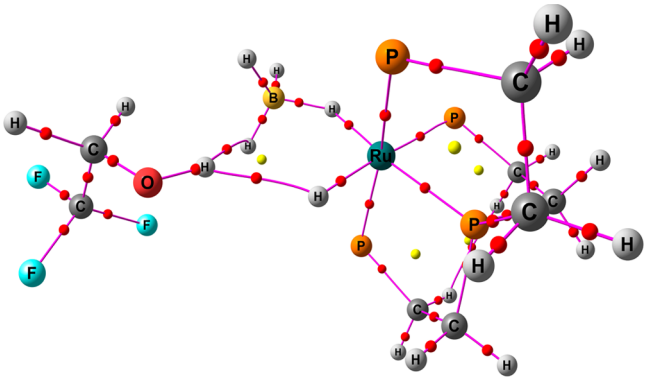

Figure 4. Molecular graphs of DHB complex **2**·TFE_**IIIac**. Methyl groups of the phosphorus ligand are omitted for clarity. Color coding: red spheres—(3; −1) critical points, yellow spheres—(3; +1) critical points.

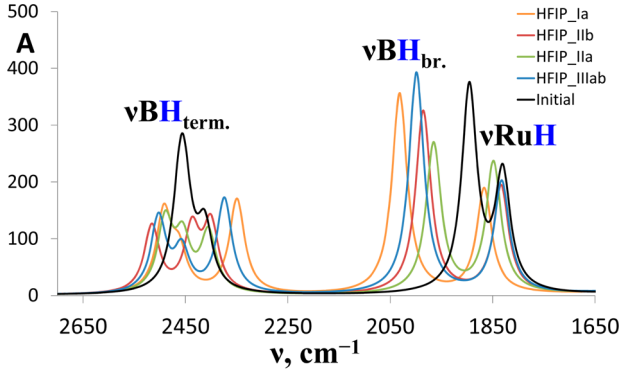

Figure 5. Calculated IR spectra of complex **2** and the DHB complexes **2**·HFIP (**Ia**, **IIa**, **IIb**, **IIIab**).

(200 K) could be taken as a rough estimation of the $T_{1\ min}$(BH) time.

The low-temperature addition (200 K) of a 3-fold excess of HFIP to complex **1** causes spectral changes only in the BH_4^- region. Thus, the resonance of the BH bridge observed at 190 K disappears, and a broadened line appears at −1.6 ppm. This resonance, integrating to 4 protons, is assigned to the BH_4^- group undergoing the bridge-terminal exchange, which is faster than it is in the initial complex **1**. A mechanism accounting for the acceleration of the dynamic process in the presence of the proton donor remains unclear, but the observed effect provides the correct T_1 measurements for the RuH and BH_4^- signals between 240 and 190 K. We have found that the T_1 time of both signals passes through a minimum at 210 K: $T_{1\ min}$(RuH) = 0.166 s and $T_{1\ min}$(BH) = 0.10 s. Thus, the presence of HFIP leads to the increase of the temperature of the $T_{1\ min}$ observation by ca. 10 degrees because of an increase of the inertia moment of complex **1**. This fact clearly supports the formation of an intermolecular adduct between complex **1** and the alcohol. However, in the presence of HFIP, the chemical shift of the Ru hydride resonance does not practically change [δ = −8.933 ($\Delta\delta$ = +0.06) and −8.901 ($\Delta\delta$ = +0.08) ppm at 240

dx.doi.org/10.1021/ic4026206 | Inorg. Chem. 2014, 53, 1080−1090

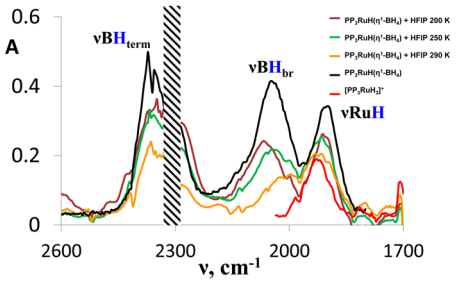

Figure 6. IR spectra in the ν_{MH} region: complex **1** (0.020 M, black line) at 200 K; complex **1** (0.025 M) + 2 equiv of HFIP (0.056 M) at 200 K (maroon line), 250 K (green line), and 290 K (orange line); $[(PP_3)RuH_{eq}(\eta^2\text{-}H_2)]^+[BF_4]^-$ (red line)[39] obtained in situ by the reaction between $(PP_3)RuH_2$ and 1 equiv of HBF_4 (0.023 M). CH_2Cl_2, l = 1.2 mm. Shaded area denotes the region masked by the CH_2Cl_2 absorption.

and 190 K, respectively]. Also the $T_{1\,min}$ value of the RuH resonance does not significantly change in the presence of HFIP. Actually, the change in $T_{1\,min}$ from 178 to 166 ms is widely within the limits of T_1 experimental error (7%). Hence, the Ru hydride ligand is not involved in the DHB, in full agreement with the IR results.

In contrast, the decrease of the BH relaxation time on going from complex **1** ($T_{1\,min}$(BH) = 0.13 s) to the H-bonded complex with HFIP ($T_{1\,min}(BH)^{DHB}$ = 0.10 s) may be likely ascribed to the additional hydride−proton dipole−dipole interactions. This is also in agreement with the IR data, showing that complex **1** forms with the proton donors BH···HO adducts where the terminal H_{term}(B) atom acts as the proton acceptor.

Assuming that the equilibrium shown in eq 1 is completely shifted to the H-bonded adduct at low temperature and taking into account the fast exchange of BH_4^- hydrogens, we may calculate by eq 4 the value of $T_{1\,min}^{obs}$ (BH···HO) = 0.06 s, for one of the four borohydride ligands H-bonded to the alcohol.

$$\frac{1}{T_{1\min}(\mathrm{BH})^{\mathrm{exp}}_{\mathrm{DHB}}} = \frac{3}{4}\frac{1}{T_{1\min}(\mathrm{BH})^{\mathrm{free}}} + \frac{1}{4}\frac{1}{T^{\mathrm{obs}}_{1\min}(\mathrm{BH}\cdots\mathrm{HO})} \quad (4)$$

The hydride−proton distance $r_{(H...H)}$ may be therefore estimated via eq 5[64] to be 1.7 Å, which is remarkably less than 2.4 Å and is comparable to the H···H lengths found for other DHB complexes.[30,31,39,65,66]

$$r_{(\mathrm{H}\cdots\mathrm{H})} = 5.815\left(\frac{1}{T^{\mathrm{obs}}_{1\min}(\mathrm{BH}\cdots\mathrm{HO})} - \frac{1}{T_{1\min}(\mathrm{BH})^{\mathrm{free}}}\right)^{-1/6}\nu^{-1/6} \quad (5)$$

Thus, a combination of VT IR and NMR spectral studies allowed us to observe DHB complexes (BH_{term}···HOR) with different proton donors and to determine the thermodynamic and metrical (H···H distance) parameters of those complexes.

Theoretical Investigations of DHB Complexes. To get a deeper insight into the electronic structures and properties (electron density distribution, frequencies of BH stretching vibrations and interaction energies) of DHB complexes, theoretical calculations were run for adducts of proton donors

Scheme 1. Coordination Modes [Mono- (I), Bi- (II), and Tridentate (III)] in DHB Complexes[a]

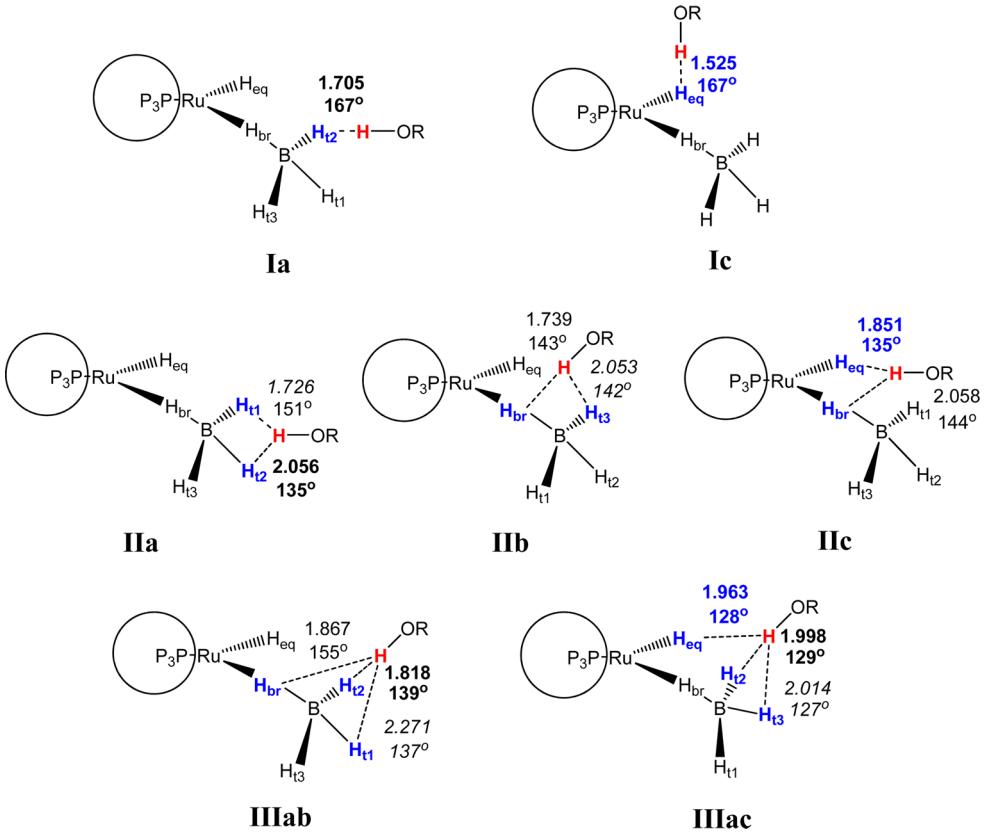

[a]The contact lengths (Å) and corresponding OH···H angles (in degrees) are indicated as H_{eq}···H (blue bold), H_{br}···H (regular), H_{t1}···H (italic), H_{t2}···H (bold) for the optimized **2**·HFIP adducts.

dx.doi.org/10.1021/ic4026206 | Inorg. Chem. 2014, 53, 1080−1090

of different strength (MeOH, TFE, HFIP) with the model complex (κ^4-P($CH_2CH_2PMe_2$)$_3$)RuH(η^1-BH_4) (**2**) in which the six phenyl groups in the PP_3 ligand are replaced by methyl groups (Supporting Information, Figure S1). This substitution does not have meaningful effect on the initial hydride geometry, as the optimized structures of complexes **1** and **2** do not differ by more than 0.07 Å for Ru−P bond distances and 0.02 Å for both the Ru−H and B−H bond distances. The variety of DHB complexes formed by proton donors with complexes **1** and **2** is found to be the same, producing similar geometry, which validates the use of complex **2** as a model. (For example, for the **IIIac**_TFE complex, the length of the primary H···H contact (see below) increases by 0.04 Å when passing from complex **2** to complex **1**, while secondary contacts differ by less than 0.1 Å.)

Structural Analysis. Unlike the metal η^2-tetrahydroborate complexes, where the BH_4 group is a distorted tetrahedron of C_s local symmetry,[24,31] in complexes **1** and **2** the BH_4 substituent adopts a distorted trigonal pyramidal geometry. Consequently, the DHBs with the proton donors (Scheme 1, Supporting Information, Figure S2) are formed not only at its vertexes (monodentate complexes, **Ia**) or edges (bifurcate complexes, **IIa** and **IIb**), but they may also involve a triangular face (complex **IIIab**) [trifurcate complexes which were not found in the previously studied case of (Ph_3P)$_2$Cu(η^2-BH_4)].[31] Three other types of DHB adducts are represented by the complexes with the additional interaction to RuH (complexes **Ic**, **IIc**, and **IIIac**, Scheme 1, Supporting Information, Figure S2). Thus, all the hydride centers (RuH, BH_{term}, and BH_{br}) can be involved in DHB formation; a higher number of potential coordination centers leads to an increased variety of DHB complexes formed by complex (PP_3)RuH(η^1-BH_4) if compared with complex (Ph_3P)$_2$Cu(η^2-BH_4).

Monodentate DHB complexes (**Ia** and **Ic**) feature a short BH···HO contact between 1.525 and 1.748 Å, with a nearly linear arrangement of the O−H···H unit (162−177°; Supporting Information, Table S1) for all the three alcohols. These distances are in good agreement with $r_{(H\cdots H)}$ determined from $T_{1\ min}$ (1.7 Å) and fall in the typical range of DHBs involving boron hydrides.[31,35,36,61,66] Almost similar lengths are found in DHB complexes of BH_4^- with the same proton donors (1.553−1.654 Å).[61] The H···H distance in all cases shortens with the increase of the proton donor strength.

Bifurcate DHB complexes (**IIa**, **IIb**, and **IIc**) feature two H··· HO contacts—primary and secondary.[31] The primary (shortest) contact is longer than in monodentate complexes (1.718−1.974 Å; Supporting Information, Table S1). The secondary interactions feature significantly longer H···H distances of 2.026−2.237 Å. The angles are far from 180° in all cases, and their values decrease from primary to secondary contacts and from complexes **IIa**−**IIb** to complex **IIc** (Supporting Information, Figure S2 and Table S1). Formation of one more contact (to BH_{br} or RuH) transforms complex **IIa** into complexes **IIIab** and **IIIac**—the trifurcate DHB complexes.

Upon DHB formation the O−H bonds of proton donors elongate by 0.011−0.018 Å for all DHB complexes except complex **Ic**, where O−H bonds are significantly longer (Δr_{OH} = 0.021−0.038 Å; Supporting Information, Table S2). The B−H_{term} bonds participating in the interaction elongate by 0.002−0.012 Å. Both Ru−H_{br} and B−H_{br} show a nonspecific response to the DHB formation (Supporting Information, Table S2) that prevents their use for the effective assignment of spectral data. The potential energy surface for the (PP_3)RuH(BH_4)·HOR adducts is rather flat, and their energies vary in a quite narrow range of a few kcal/mol (*vide infra*), forcing us to consider several factors to find the best fit to the experiment.

Electron-Density Analysis. Mapping the molecular electrostatic potential of complex **2** reveals an electron density area located on the BH_4^- fragment, with two minima at V_{min} = −50.8 and −53.5 kcal/mol (Figure 3). This result corresponds to the substantial involvement of BH_{term} ligands in the interaction with proton donors, already evident from the structural parameters.

The electron density redistribution, which occurs upon DHB formation, was analyzed using different approaches, namely, natural population analysis (NPA),[50] WBIs,[49] and Bader's theory "atoms in molecules" (AIM).[54−56] As expected, the charge on the HOR proton becomes more positive, whereas that on the interacting hydridic hydrogen(s) becomes more negative (Supporting Information, Table S3).

Within the framework of the AIM theory, a hydrogen bond is characterized by the presence of the (3; −1) critical point that allows one to distinguish it from other types of interaction.[67] Despite the presence of several short intermolecular OH···HB contacts in most of the **2**·HOR adducts, the (3; −1) critical point (Supporting Information, Figures S3−S5) was found only for the closest contact with the most linear O−H···H(B) arrangement. The presence of additional interactions causes deviation of the hydrogen bond geometry from linearity, which is reflected in the values of the H···H bond ellipticity (Supporting Information, Table S4).

In the trifurcate complexes **IIIac**, where two hydride ligands of different nature (RuH and BH_{term}) participate in the binding to the alcohol, two critical points were found corresponding to the RuH···H(O) and BH_{term}···H(O) DHBs (Figure 4). The (3; +1) critical point of the six-membered (O)H···H−B−H−Ru−H···H(O) cycle confirms the formation of a double dihydrogen bonded structure.

In complexes **IIc**, where RuH and BH_{br} ligands are involved in the bonding, two (3; −1) critical points were found only in the case of TFE (Supporting Information, Figure S4). In addition, the (3; +1) critical point of four-membered cycle (O)H···H−Ru−H···H(O) is found close to the (3; −1) critical point of the O−H···H_{br}(B) bond. This indicates the structural instability and increased probability of opening the cycle as indeed happens in case of complexes **IIc** with MeOH and HFIP (see Supporting Information, Figure S4).

The strength of the primary H···H interaction increases for stronger proton donors, as can be seen from the values of the electron density at the (3, −1) bond critical point of the H···H contact (ρ_c). The ρ_c values range from 0.010 to 0.033 au, being in the range typical for hydrogen bonds (0.004−0.178 au) (Supporting Information, Table S4).[68]

The electron density shift that takes place during the DHB formation was analyzed using the relative contribution of the σ_{BH} and σ_{MH} to σ^*_{OH} donation energy estimated from 2nd-order perturbative analysis of donor−acceptor interactions as implemented in NBO.[28,29] Typically, the hydrogen bond entails the transfer of electron density from the HOMO orbital of the base to an empty σ^*_{X-H} orbital of the acid. In all the complexes analyzed herein, the main $\sigma_{base}\rightarrow\sigma^*_{OH}$-donation corresponds to the shortest H···H contact; the impact of the secondary interactions vary from 9 to 37% of the total donation energy from base to acid (Supporting Information, Table S5). Notably, the donation from the d-pairs of ruthenium does not exceed 1

dx.doi.org/10.1021/ic4026206 | *Inorg. Chem.* 2014, 53, 1080−1090

kcal/mol in all complexes, evidencing the absence of proton donor interaction with the metal atom.[42,69]

Frequency Analysis. All four of the BH stretching vibrations in complex $(PP_3)RuH(\eta^1\text{-}BH_4)$ are IR-active. Three stretching vibrations of the terminal BH bonds (two $\nu_{BH_{term}}{}^{as}$ and one $\nu_{BH_{term}}{}^{s}$) were calculated for complex **2** at 2460, 2452, and 2414 cm^{-1}, respectively; the stretching vibration of the bridging BH bond (ν_{BHbr}) was found at 1895 cm^{-1}, and the RuH stretching vibration (ν_{RuH}) at 1830 cm^{-1}. The frequency analysis for the real molecule **1** gives two $\nu_{BH_{term}}{}^{as}$ and one $\nu_{BH_{term}}{}^{s}$ at 2494, 2468, and 2414 cm^{-1} and $\nu_{BH_{br}}$ and ν_{RuH} at 2080 and 1932 cm^{-1} (Supporting Information, Table S6). Computed frequencies of the real compound **1** are only slightly higher than the experimental ones, providing a satisfactory description of the vibrational spectra. The difference between $\nu_{BH_{term}}$ in complexes **1** and **2** is only 34 cm^{-1}, while for ν_{BHbr} and ν_{RuH} it raises to 185 cm^{-1}. Nevertheless, the bands relative positions do not change when passing from complex **1** to complex **2**, keeping $\nu_{BH_{br}}$ always at higher frequencies than the ν_{RuH}. The two high-frequency $\nu_{BH_{term}}{}^{as}$ vibrations coalesce to one band in both CD_2Cl_2 solution and nujol mull; the same behavior could be observed with the simulated spectra when line-broadening is applied (Supporting Information, Figure S6). The frequency difference between the center of the $\nu_{BH_{term}}{}^{as}$ doublet and $\nu_{BH_{term}}{}^{s}$ is similar in both the real compound and the calculated model (70 cm^{-1} (experiment), 67 cm^{-1} (for complex **1**) and 42 cm^{-1} (for complex **2**)).

The most significant changes in the IR spectra of dihydrogen-bonded complexes of boron hydrides are observed in the ν_{OH} and ν_{BH} regions.[43] The frequency analysis of DHB adducts (Supporting Information, Tables S7–S9 and Figures S7–S9) shows that only the complexes with a predominant interaction through their BH_{term} proton (**Ia**, **IIa**, **IIb**, and **IIIab**) conform to the experimental observations for ν_{BH} frequencies. These complexes give a low-frequency shift of ν_{BHterm} ($\nu_{BH_{term}}{}^{as}$ and $\nu_{BH_{term}}{}^{s}$ from −63 to −7 cm^{-1}), a high-frequency shift of $\nu_{BH_{term}}{}^{as}$ from 3 to 55 cm^{-1}, and a high-frequency shift of $\nu_{BH_{br}}$ and ν_{RuH} of 70–136 cm^{-1} and 2–36 cm^{-1}, respectively. (For an example with HFIP see Figure 5.) Note, complexes **Ia** and **IIa** should provide a high-frequency ν_{RuH} shift that was not observed experimentally, so complexes **IIb** and **IIIab** give the best fit with the experiment.

Interaction Energies. The formation energies determined as the energy difference between the adduct and the isolated reactants as well as the energies of DHB derived from AIM ($E_{H\cdots H} = 0.5 \times V(r)$) are gathered in Table 2 (example of complex **2** interacting with HFIP). The data for other alcohols are summarized in the Supporting Information (Table S10). When basis set superposition error (BSSE) correction was taken into account, a significant lowering of the complexation energy (up to 36%) was observed, especially for HFIP. The inclusion of nonspecific solvent effects (CH_2Cl_2) lowers the complex formation energy by ca. 35%, but this does not change the relative stability of the complexes (ΔE_{DCM}; Supporting Information, Table S10).

Table 2. Formation Energy for DHB Complexes of 2·HFIP (kcal/mol) and Energy H···H Bond Critical Point ($E_{H\cdots H}$)

complex	ΔE	ΔE_{ZPVE}	ΔE_{BSSE}	ΔE_{DCM}	$E_{H\cdots H}$
Ia_HFIP	−24.3	−21.8	−16.7	−14.5	−4.0
Ic_HFIP	−19.6	−15.5	−12.4	−11.1	−6.1
IIa_HFIP	−23.5	−22.2	−17.3	−16.4	−4.4
IIb_HFIP	−25.4	−23.1	−19.3	−16.4	−4.9
IIc_HFIP	−24.9	−22.9	−18.4	−15.1	−2.9
IIIab_HFIP	−24.7	−22.7	−19.2	−16.2	−4.9
IIIac_HFIP	−21.5	−19.3	−15.8	−14.3	−3.2/−2.0

Among the DHB complexes modeled through these quantum-chemical calculations, those with predominant coordination of the proton donor to BH_{term} ligand are the most energetically favorable. This finding confirms the conclusion made on the basis of frequency calculations: the complexes **IIb** or **IIIab** should be the forms found experimentally. However, the formation energies of complexes **IIa** and **IIc** differ by just few tenths of kcal/mol (Table 2), and their formation could not be excluded on this basis. However, it can be excluded on the basis of the frequency analysis (vide supra).

Reaction Mechanism. *Experimental Study.* As mentioned in the Introduction, the protonation of complex $(PP_3)RuH(\eta^1\text{-}BH_4)$ (**1**) by sulfuric acid in tetrahydrofuran (THF) leads to the η^2-H_2 complex, where dihydrogen occupies the axial position trans to the apical phosphorus atom of PP_3 ligand. The hydrido(η^2-H_2) complex was isolated as the BPh_4 salt, and the X-ray structure was determined.[38] So, we could assume that protonation by weaker acids such as alcohols also yields the cationic hydrido(dihydrogen) complex $[(PP_3)RuH_{eq}(\eta^2\text{-}H_2)]^+[BH_{(3-n)}(OR)_n]^-$ (eq 6).

$$(PP_3)RuH(\eta^1\text{-}BH_4) + n\mathrm{HOR} \rightarrow [(PP_3)RuH_{eq}(\eta^2\text{-}H_2)]^+[BH_{(3-n)}(OR)_n]^- + n\mathrm{H_2} \quad (6)$$

Interestingly, the proton transfer from fluorinated alcohols to the parent dihydride $(PP_3)RuH_2$, as has been shown in our previous study, leads to the same cationic dihydrogen complex $[(PP_3)RuH_{eq}(\eta^2\text{-}H_2)]^+$ via DHB complexes to H_{ax}.[39]

Protonation of complex **1** by TFA and fluorinated alcohols (TFE, HFIP, PFTB) was studied experimentally in the same low polar solvent (CH_2Cl_2). In the case of TFA, the reaction proceeds in 20–30 min even at low temperature (200 K) (Supporting Information, Figure S10), but in the case of alcohols it is observed only above 250 K. The IR spectral pattern dramatically changes upon gradual warming from 250 K to 290 K (Figure 6): high-frequency shifts of ν_{RuH} significantly increase to 10–19 cm^{-1}, whereas low-frequency shifts of $\nu_{BH_{term}}$ are found for both $\nu_{BH_{term}}{}^{as}$ (4–8) cm^{-1} and $\nu_{BH_{term}}{}^{s}$ (16–24) cm^{-1} (Supporting Information, Tables S11 and S12). At 250 K, the $\nu_{BH_{br}}$ band decreases in intensity about 2 times and shifts to lower frequencies (by 5–17 cm^{-1}), suggesting that the B–H_{br} unit becomes the proton-accepting site and that its amount decreases due to the rupture of this bond. At room temperature this band almost disappears. Decrease in the intensity of $\nu_{BH_{term}}$ is significantly less pronounced. The proton transfer leads to formation of $[(PP_3)RuH_{eq}(\eta^2\text{-}H_2)]^+$ cation as confirmed by the appearance of a new band at 1930 cm^{-1} assigned to ν_{RuH} vibration in this cation (Figure 6 and Supporting Information, Figure S10).[39]

Thus, we can postulate that the proton transfer occurs via the acid-mediated dissociation of the B–H_{br} bond. The proton-transfer reaction proceeds slowly at low temperature and

dx.doi.org/10.1021/ic4026206 | Inorg. Chem. 2014, 53, 1080–1090

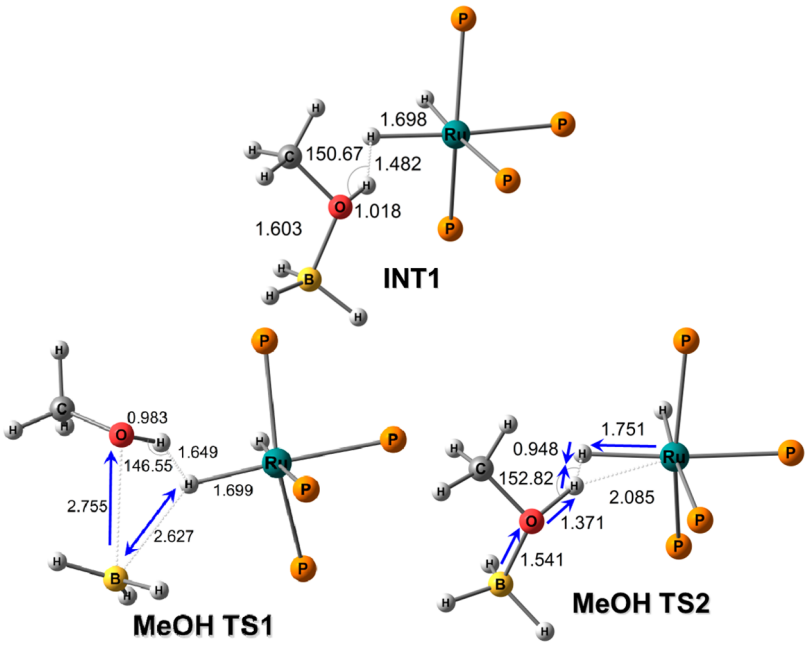

Figure 7. DFT/M06-optimized structure of complexes **INT1**, **TS1**, and **TS2** for the reaction of complex **2** with MeOH. Methyl groups and ethylene bridges of the phosphorus ligand are omitted for clarity.

accelerates on warming to room temperature. The protonated $[(PP_3)RuH_{eq}(\eta^2\text{-}H_2)]^+$ species forms with all proton donors.

DFT Study of Proton Transfer to BH Ligands. In quantum-chemical calculations, two possible pathways for proton transfer were considered: to the B−H and Ru−H sites (the energy values on the profiles reported on the Figures 8 and 10 are given for the gas-phase-optimized geometries). The first pathway is in good agreement with the experimental data, in which the evidence of the DHB complex with BH_{term} site was found. In the case of weak acids (MeOH, TFE) the bifurcate dihydrogen-bonded complex is the first reaction intermediate (**IIa**_TFE or **IIb**_MeOH). The proton transfer is preceded by the B−H_{br} bond dissociation, yielding complex **INT1** (Figure 7). The calculated activation barrier of this stage is 27.5 and 28.2 kcal/mol for MeOH and TFE, respectively (complex **TS1**, Figure 7). From the literature data it is known that this bond is labile and readily dissociates under low vacuum or in the presence of rather weak bases.[38] The oxygen atom of weak proton donors is sufficiently basic to afford BH_3 stabilization through B−O coordination (Figure 7, right). Yet another benefit from the formation of the RO(H)···BH_3 adduct is the increase of the alcohol strength due to the electron-withdrawing effect of the BH_3 group. The proton transfer from the RO(H)···BH_3 moiety to the former RuH_{br} ligand proceeds via complex **TS2** (Figure 7) with very low barriers (6.0 kcal/mol for MeOH and 0.7 kcal/mol for TFE). The reaction product is the $[(PP_3)RuH_{eq}(\eta^2\text{-}H_2)]^+[BH_3OR]^-$ ion pair, in which the η^2-H_2 ligand occupies the axial position trans to the apical phosphorus atom of PP_3, matching the structure shown experimentally.[38,39] For such a pathway, the energies of all intermediates and transition states are lower for TFE than they are for MeOH (Figure 8). Also, the energies of the proton-transfer products are below those of the reactants but above those of the DHB intermediate. This suggests that the MeOH and TFE reactions would not proceed past the DHB complex; however, the irreversible $[H_3BOR]^-$ formation could pull the proton-transfer reaction.

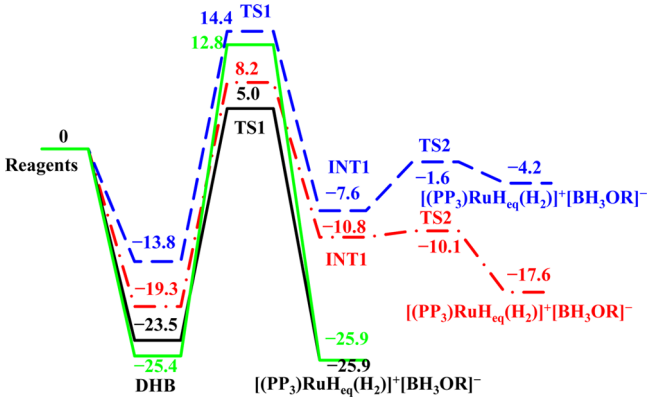

Figure 8. Energy profile (ΔE, in kcal/mol) for the reaction of complex **2** with ROH with the interaction on BH site (MeOH—blue dashed line, TFE—red dash-dot line, HFIP—black and green solid lines).

As mentioned above, switching from MeOH to TFE leads to practically negligible barriers for the second step ($\Delta E^{\ddagger}_2 = E_{TS2} - E_{INT1}$ = 0.7 kcal/mol). Further increase of the acid strength leads to the concerted proton transfer in one step (see Figure 8 for HFIP; Supporting Information Figure S14 for CF_3OH, Figure S15 for CF_3COOH). The active intermediate in this case is the DHB complex of type **IIb**, and the transition state shows the insertion of the proton donor into the B−H_{br} bond. Two concerted mechanisms were calculated. In the first one, the transition state $\mathbf{TS1}^{diss}_{BH}$ connects complexes **IIa** and **IIb** with the $[(PP_3)RuH_{eq}(\eta^2\text{-}H_2)]^+[BH_3OR]^-$ ion pair and is characterized by the predominant contribution of B−H_{br} bond dissociation to the TS geometry, so we name it "*dissociation pathway*" (Figure 9 left). Another transition state, $\mathbf{TS1}^{PT}_{BH}$, connects complexes **IIb** with the same $[(PP_3)RuH_{eq}(\eta^2\text{-}H_2)]^+[BH_3OR]^-$ ion pair, but its main feature is the occurrence of the O−H bond dissociation accompanied by the H−H ligand formation ("*proton-transfer pathway*," Figure 9 right).

dx.doi.org/10.1021/ic4026206 | *Inorg. Chem.* 2014, 53, 1080−1090

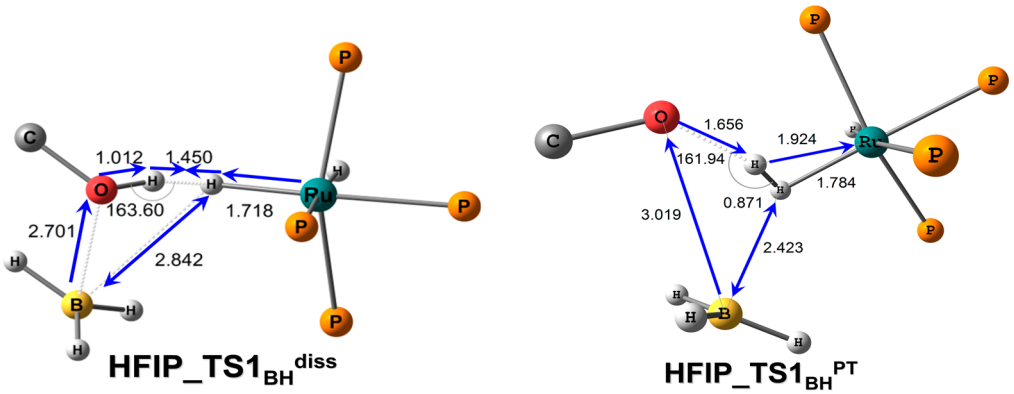

Figure 9. DFT/M06-optimized structures of complexes $\mathbf{TS1}_{BH}^{diss}$ and $\mathbf{TS1}_{BH}^{PT}$ for the reaction of complex **2** with HFIP. Methyl groups and ethylene bridges of the phosphorus ligand as well as the substituents at the α carbon of the alcohol are omitted for clarity.

Complexes of type **IIIab** can be regarded as a sort of overlap between complexes **IIa** and **IIb**; thus, they can be taken as starting point for both dissociation and proton-transfer pathways, especially for the strongest proton donors, which are prone to multiple interactions. Nevertheless, none of our IRC calculations revealed a connection of **IIIab** complexes to transition states $\mathbf{TS1}_{BH}^{diss}$ and $\mathbf{TS1}_{BH}^{PT}$.

For all proton donors, the dissociation pathway (via comlpex $\mathbf{TS1}_{BH}^{diss}$) is more favorable, but the difference ($\Delta\Delta E^{\ddagger}$) in activation energy of the two concerted mechanisms decreases from 9.7 to 3.8 kcal/mol when increasing the acidity of the proton donor from HFIP to TFA (Table 3).

Table 3. The Activation Energy ($\Delta E^{\ddagger} = E_{TS} - E_{DHB}$, kcal/mol) for Different Pathways of the Reaction of Complex 2 with Strong Proton Donors (HFIP, Trifluoromethanol, and TFA)

	HFIP	TFM	TFA
$\mathbf{TS1}_{BH}^{diss}$	28.4	19.8	17.4
$\mathbf{TS1}_{BH}^{PT}$	38.2	25.0	21.2
$\mathbf{TS1}_{RuH}$	11.8	2.1	3.2

DFT Study of Proton Transfer to RuH_{eq} Site. The active intermediate of the proton transfer to the Ru–H_{eq} site (Figure 10) is a monodentate DHB complex of type **Ic**, which is energetically less favorable than complexes **IIa** and **IIb.** Despite the rather short Ru–H···H–O contacts, in complexes **IIc** and **IIIac** no proton transfer to the RuH site occurs, probably because of an unsuitable OH group orientation.

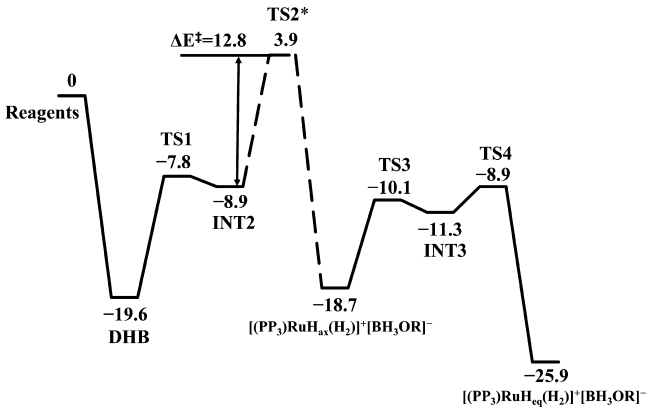

Figure 10. Energy profile for the reaction of complex **2** with HFIP with interaction at RuH site (ΔE in kcal/mol).

The activation barrier of proton transfer to the RuH_{eq} site is significantly lower ($E_{TS1} - E_{DHB(Ic)}$ = 11.8 kcal/mol for HFIP) than those associated with the transition states $\mathbf{TS1}_{BH}^{PT}$ and $\mathbf{TS1}_{BH}^{diss}$ (38.2 and 28.5 kcal/mol, respectively). This value is comparable to that obtained for the protonation of $(PP_3)RuH_2$ (the activation barrier $\Delta E^{\ddagger}$ for proton transfer from HFIP to RuH_{eq} site equals 10.2 kcal/mol, Supporting Information, Figure S18). The ion pair $[(PP_3)Ru(\eta^1\text{-}HBH_3)(\eta^2\text{-}H_2)]^+[OR]^-$ (**INT2**) formed after proton transfer to the RuH_{eq} site in complex **2** has an η^2-H_2 ligand at the equatorial position, and dissociation of B–H_{br} bond is still required (Supporting Information, Figure S16).

One could suggest that dissociation of the B–H_{br} bond proceeds in a similar manner as in the case of the above-described dissociative concerted mechanism. To model the B–H_{br} bond breaking in the $[(PP_3)Ru(\eta^1\text{-}HBH_3)(\eta^2\text{-}H_2)]^+[OR]^-$ ion pair, the external THF molecule was used as a base (Supporting Information, Figure S17). This gave complex **TS2*** 12.8 kcal/mol above complex **INT2·THF** (Figure 9). The relocation of the BH_3 fragment from the external base to the HFIP anion proceeds as low-barrier dissociation–association and results in the ion pair $[(PP_3)RuH_{ax}(\eta^2\text{-}H_2)]^+[BH_3OR]^-$ (Supporting Information, Figure S15), which still has η^2-H_2 ligand in the equatorial position. Its isomerization to the thermodynamically stable product $[(PP_3)\text{-}RuH_{eq}(\eta^2\text{-}H_2)]^+[BH_3OR]^-$ occurs rather easily via movement of the $[BH_3OR]^-$ anion and hydride exchange (complexes **TS3**, **TS4**) between the classical and nonclassic hydride sites. The latter scrambling is well documented for $MH(\eta^2\text{-}H_2)$ complexes.[70−73] The calculated activation barrier of the hydride exchange is −11.0 kcal/mol, which is close to the value of $\Delta G^{\ddagger}_{exp}$= 12.1 ± 0.3 kcal/mol obtained experimentally for the $[(PP_3)RuH_3]^+$ cation.[38]

The key step for this pathway is proton transfer to the RuH_{eq} site followed by the B–H_{br} bond dissociation. The formation of complex **INT2** virtually assists the climbing to the highest transition state of the process. The effective activation barrier of the proton transfer to the RuH site could be estimated as the difference between the energy at the highest point (complex **TS2***) and the energy of the DHB intermediate. This value (23.5 kcal/mol) is only slightly lower (by ca. 5 kcal/mol) than that for the concerted proton transfer from HFIP via complex $\mathbf{TS1}_{BH}^{diss}$.

dx.doi.org/10.1021/ic4026206 | Inorg. Chem. 2014, 53, 1080−1090

Thus, although this pathway starts from the less favorable DHB complex with RuH ligand and leads to a product which needs further isomerization, it features lower activation barriers that make this mechanism feasible. Interconversion between the DHB complexes of different types should be easy as well, since their energies vary within 2 kcal/mol in most cases (Table 2 and Supporting Information, Table S10). For strong acids (like TFA) almost barrierless proton transfer to RuH could be envisaged as the operative pathway. The $B-H_{br}$ bond breaking appears to be the common key step of all pathways studied.

CONCLUSION

With its five different hydride ligands, the complex $(PP_3)RuH(\eta^1\text{-}BH_4)$ may form various types of DHB complexes. The most stable of them features an interaction of the proton donor with the terminal BH ligands, as proved by low-temperature (200−230 K) IR and NMR experiments. The proton transfer proceeds slowly at low temperature and speeds up upon warming to ambient temperature. DFT/M06 quantum-chemical calculations show that DHB complexes are active intermediates of the proton-transfer reaction: bifurcate DHB complexes **IIa** and **IIb** precede the protonation of the BH site and the **Ic**-protonation of the RuH site. Proton transfer via DHB with BH_{term} ligands starts from the most stable complexes and leads to the thermodynamic reaction product, but rather high barriers were found for all the alcohols considered in this study (27−30 kcal/mol for MeOH, TFE, HFIP). DFT calculations show that the protonation at the RuH site is kinetically preferable (the barrier found for HFIP is ca. 23 kcal/mol), even if it starts from a higher-energy intermediate and results in a protonation product which has to undergo further isomerization to give the final product $[(PP_3)RuH_{eq}(H_2)]^+[BH_3OR]^-$. Both pathways are feasible, since the interconversion between the DHB complexes of different types should be easy, especially at ambient temperature. The $B-H_{br}$ bond breaking appears to be the common key step of all pathways studied. These data provide an alternative pathway for the activation of hydrido-borohydride precatalysts in protic solvents,[14,15,74,75] which generates catalytically active $M(\eta^2\text{-}H_2)$ species and OR-base (instead of M(ROH) or M(OR) complexes) as the result of proton transfer and $B-H_{br}-M$ bond breaking. Further studies are in progress in our laboratories to elucidate the influence of different factors (e.g., nature of both metal and ligand) on this reaction mechanism.

ASSOCIATED CONTENT

Supporting Information

The manuscript was written through contributions of all authors. All authors have given approval to the final version of the manuscript.

This material is available free of charge via the Internet at http://pubs.acs.org.

AUTHOR INFORMATION

Corresponding Authors

*E-mail: shu@ineos.ac.ru. Fax: +7 499 1355085. (E.S.S.)
*E-mail: maurizio.peruzzini@iccom.it. Fax: +39 055 5225 203. (M.P.)

Notes

The authors declare no competing financial interest.

ACKNOWLEDGMENTS

The work was supported by the Russian Foundation for Basic Research (RFBR, Projects 13-03-00604, 12-03-33018 and 12-03-31176), GDRI, *"Catalyse Homogène pour le Développement Durable (CH2D)* and CNR-RAS bilateral agreement.

REFERENCES

(1) Sorrell, T. N. *Tetrahedron Lett.* **1978**, *19*, 4985−4986.
(2) Sorrell, T. N.; Pearlman, P. S. *J. Org. Chem.* **1980**, *45*, 3449−3451.
(3) Fleet, G. W. J.; Harding, P. J. C.; Whitcombe, M. J. *Tetrahedron Lett.* **1980**, *21*, 4031−4034.
(4) Fleet, G. W. J.; Harding, P. J. C. *Tetrahedron Lett.* **1981**, *22*, 675−678.
(5) Bhattacharyya, S.; Chatterjee, A.; Williamson, J. S. *Synth. Commun.* **1997**, *27*, 4265−4274.
(6) Ravikumar, K. S.; Sinha, S.; Chandrasekaran, S. *J. Org. Chem.* **1999**, *64*, 5841−5844.
(7) Zeynizadeh, B. *Bull. Chem. Soc. Jpn.* **2003**, *76*, 10.
(8) Bhanushali, M. J.; Nandurkar, N. S.; Bhor, M. D.; Bhanage, B. M. *Tetrahedron Lett.* **2007**, *48*, 1273−1276.
(9) Firouzabadi, H.; Iranpoor, N.; Alinezhad, H. *J. Iran. Chem. Soc.* **2009**, *6*, 177−186.
(10) Bianchini, C.; Ghilardi, C. A.; Meli, A.; Midollini, S.; Orlandini, A. *Inorg. Chem.* **1985**, *24*, 924−931.
(11) Jensen, J. A.; Gozum, J. E.; Pollina, D. M.; Girolami, G. S. *J. Am. Chem. Soc.* **1988**, *110*, 1643−1644.
(12) James, B. D.; Nanda, R. K.; Walbridge, M. G. H. *Inorg. Chem.* **1967**, *6*, 1979−1983.
(13) Hori, J.; Murata, K.; Sugai, T.; Shinohara, H.; Noyori, R.; Arai, N.; Kurono, N.; Ohkuma, T. *Adv. Synth. Catal.* **2009**, *351*, 3143−3149.
(14) Zhang, J.; Balaraman, E.; Leitus, G.; Milstein, D. *Organometallics* **2011**, *30*, 5716−5724.
(15) Langer, R.; Iron, M. A.; Konstantinovski, L.; Diskin-Posner, Y.; Leitus, G.; Ben-David, Y.; Milstein, D. *Chem.—Eur. J.* **2012**, *18*, 7196−7209.
(16) Grutsch, P. A.; Kutal, C. *J. Am. Chem. Soc.* **1977**, *99*, 6460−6463.
(17) Murray, R. E. U.S. Patent No. 4,822,915, 1989.
(18) Mahrova, T. V.; Fukin, G. K.; Cherkasov, A. V.; Trifonov, A. A.; Ajellal, N.; Carpentier, J.-F. *Inorg. Chem.* **2009**, *48*, 4258−4266.
(19) Visseaux, M.; Bonnet, F. *Coord. Chem. Rev.* **2011**, *255*, 374−420.
(20) Nakayama, Y.; Watanabe, N.; Kusaba, K.; Sasaki, K.; Cai, Z.; Shiono, T.; Tsutsumi, C. *J. Appl. Polym. Sci.* **2011**, *121*, 2098−2103.
(21) Kratsch, J.; Kuzdrowska, M.; Schmid, M.; Kazeminejad, N.; Kaub, C.; Oña-Burgos, P.; Guillaume, S. M.; Roesky, P. W. *Organometallics* **2013**, *32*, 1230−1238.
(22) Marks, T. J.; Kolb, J. R. *Chem. Rev.* **1977**, *77*, 263−293.
(23) Makhaev, V. D. *Russ. Chem. Rev.* **2000**, *69*, 727.
(24) Besora, M.; Lledós, A. Coordination Modes and Hydride Exchange Dynamics in Transition Metal Tetrahydroborate. In *Complexes Contemporary Metal Boron Chemistry I*; Marder, T.; Lin, Z., Eds.; Springer: Berlin/Heidelberg: 2008; Vol. *130*, pp 149−202.
(25) Rossin, A.; Peruzzini, M.; Zanobini, F. *Dalton Trans.* **2011**, *40*, 4447−4452.
(26) Crabtree, R. H.; Siegbahn, P. E. M.; Eisenstein, O.; Rheingold, A. L.; Koetzle, T. F. *Acc. Chem. Res.* **1996**, *29*, 348−354.
(27) Peruzzini, M.; Poli, R. *Recent Advances in Hydride Chemistry*; Elsevier Science: Amsterdam, 2002.
(28) Epstein, L. M.; Shubina, E. S. *Coord. Chem. Rev.* **2002**, *231*, 165−181.
(29) Belkova, N. V.; Shubina, E. S.; Epstein, L. M. *Acc. Chem. Res.* **2005**, *38*, 624−631.
(30) Belkova, N. V.; Epstein, L. M.; Shubina, E. S. *Eur. J. Inorg. Chem.* **2010**, *2010*, 3555−3565.
(31) Golub, I. E.; Filippov, O. A.; Gutsul, E. I.; Belkova, N. V.; Epstein, L. M.; Rossin, A.; Peruzzini, M.; Shubina, E. S. *Inorg. Chem.* **2012**, *51*, 6486−6497.

(32) Epstein, L. M.; Shubina, E. S.; Bakhmutova, E. V.; Saitkulova, L. N.; Bakhmutov, V. I.; Chistyakov, A. L.; Stankevich, I. V. *Inorg. Chem.* **1998**, *37*, 3013−3017.
(33) Belkova, N. V.; Filippov, O. A.; Filin, A. M.; Teplitskaya, L. N.; Shmyrova, Y. V.; Gavrilenko, V. V.; Golubinskaya, L. M.; Bregadze, V. I.; Epstein, L. M.; Shubina, E. S. *Eur. J. Inorg. Chem.* **2004**, *2004*, 3453−3461.
(34) Filippov, O. A.; Filin, A. M.; Belkova, N. V.; Tsupreva, V. N.; Shmyrova, Y. V.; Sivaev, I. B.; Epstein, L. M.; Shubina, E. S. *J. Mol. Struct.* **2006**, *790*, 114−121.
(35) Richardson, T.; de Gala, S.; Crabtree, R. H.; Siegbahn, P. E. M. *J. Am. Chem. Soc.* **1995**, *117*, 12875−12876.
(36) Custelcean, R.; Jackson, J. E. *Chem. Rev.* **2001**, *101*, 1963−1980.
(37) Filippov, O. A.; Filin, A. M.; Teplitskaya, L. N.; Belkova, N. V.; Shmyrova, Y. V.; Sivaev, I. B.; Bregadze, V. I.; Epstein, L. M.; Shubina, E. S. *Main Group Chem.* **2005**, *4*, 97−110.
(38) Bianchini, C.; Pérez, P. J.; Peruzzini, M.; Zanobini, F.; Vacca, A. *Inorg. Chem.* **1991**, *30*, 279−287.
(39) Gutsul, E. I.; Belkova, N. V.; Sverdlov, M. S.; Epstein, L. M.; Shubina, E. S.; Bakhmutov, V. I.; Gribanova, T. N.; Minyaev, R. M.; Bianchini, C.; Peruzzini, M.; Zanobini, F. *Chem.—Eur. J.* **2003**, *9*, 2219−2228.
(40) Frisch, M. J.; Trucks, G. W.; Schlegel, H. B.; Scuseria, G. E.; Robb, M. A.; Cheeseman, J. R.; Scalmani, G.; Barone, V.; Mennucci, B.; Petersson, G. A.; Nakatsuji, H.; Caricato, M.; Li, X.; Hratchian, H. P.; Izmaylov, A. F.; Bloino, J.; Zheng, G.; Sonnenberg, J. L.; Hada, M.; Ehara, M.; Toyota, K.; Fukuda, R.; Hasegawa, J.; Ishida, M.; Nakajima, T.; Honda, Y.; Kitao, O.; Nakai, H.; Vreven, T.; Montgomery, J. A.; Peralta, J. E.; Ogliaro, F.; Bearpark, M.; Heyd, J. J.; Brothers, E.; Kudin, K. N.; Staroverov, V. N.; Kobayashi, R.; Normand, J.; Raghavachari, K.; Rendell, A.; Burant, J. C.; Iyengar, S. S.; Tomasi, J.; Cossi, M.; Rega, N.; Millam, J. M.; Klene, M.; Knox, J. E.; Cross, J. B.; Bakken, V.; Adamo, C.; Jaramillo, J.; Gomperts, R.; Stratmann, R. E.; Yazyev, O.; Austin, A. J.; Cammi, R.; Pomelli, C.; Ochterski, J. W.; Martin, R. L.; Morokuma, K.; Zakrzewski, V. G.; Voth, G. A.; Salvador, P.; Dannenberg, J. J.; Dapprich, S.; Daniels, A. D.; Farkas; Foresman, J. B.; Ortiz, J. V.; Cioslowski, J.; Fox, D. J. *Gaussian 09*, Revision A.02; Gaussian, Inc.: Wallingford, CT, 2009.
(41) Zhao, Y.; Truhlar, D. *Theor. Chim. Acta* **2008**, *120*, 215−241.
(42) Wedig, U.; Dolg, M.; Stoll, H.; Preuss, H. Energy-Adjusted Pseudopotentials for Transition-Metal Elements. In *Quantum Chemistry: The Challenge of Transition Metals and Coordination Chemistry*; Veillard, A., Ed.; Springer: Netherlands: 1986; Vol. *176*, pp 79−89.
(43) Stevens, C. J.; Dallanegra, R.; Chaplin, A. B.; Weller, A. S.; Macgregor, S. A.; Ward, B.; McKay, D.; Alcaraz, G.; Sabo-Etienne, S. *Chem.—Eur. J.* **2011**, *17*, 3011−3020.
(44) Krishnan, R.; Binkley, J. S.; Seeger, R.; Pople, J. A. *J. Chem. Phys.* **1980**, *72*, 650−655.
(45) Hehre, W. J.; Ditchfield, R.; Pople, J. A. *J. Chem. Phys.* **1972**, *56*, 2257−2262.
(46) Dill, J. D.; Pople, J. A. *J. Chem. Phys.* **1975**, 62.
(47) Fritsch, J.; Zundel, G. *J. Phys. Chem.* **1981**, *85*, 556−561.
(48) Kramer, R.; Zundel, G. *J. Chem. Soc., Faraday Trans.* **1990**, *86*, 301−305.
(49) Wiberg, K. B. *Tetrahedron* **1968**, *24*, 1083−1096.
(50) Glendening, E. D.; Badenhoop, J. K.; Reed, A. E.; Carpenter, J. E.; Bohman, J. A.; Morales, C.; Weindhold, F. *Natural Bond Orbital (NBO)* 5.0; University of Wisconsin: Madison, WI, 2001.
(51) Keith, T. A. *AIMAll*, Version 11.12.19; TK Gristmill Software: Overland Park, KS, 2011.
(52) Espinosa, E.; Molins, E.; Lecomte, C. *Chem. Phys. Lett.* **1998**, *285*, 170−173.
(53) Espinosa, E.; Alkorta, I.; Rozas, I.; Elguero, J.; Molins, E. *Chem. Phys. Lett.* **2001**, *336*, 457−461.
(54) Bader, R. F. W. *Atoms in Molecules: A Quantum Theory (International Series of Monographs on Chemistry)*; Oxford University Press: New York, 1994.
(55) Popelier, P. L. *Atoms in Molecules: An Introduction*; Prentice Hall: London, 2000.
(56) Matta, C.; Boyd, R. J. *Quantum Theory of Atoms in Molecules: Recent Progress in Theory and Application*; Wiley-VCH: New York, 2007.
(57) Iogansen, A. V. *Theor. Exp. Chem.* **1973**, *7*, 249−256.
(58) Iogansen, A. V. *Theor. Exp. Chem.* **1973**, *7*, 257−261.
(59) Iogansen, A. V. *Spectrochim. Acta, Part A* **1999**, *55*, 1585−1612.
(60) Iogansen, A. V. *The Hydrogen Bond*; Nauka: Moscow, 1981.
(61) Filippov, O. A.; Filin, A. M.; Tsupreva, V. N.; Belkova, N. V.; Lledós, A.; Ujaque, G.; Epstein, L. M.; Shubina, E. S. *Inorg. Chem.* **2006**, *45*, 3086−3096.
(62) Shubina, E. S.; Bakhmutova, E. V.; Filin, A. M.; Sivaev, I. B.; Teplitskaya, L. N.; Chistyakov, A. L.; Stankevich, I. V.; Bakhmutov, V. I.; Bregadze, V. I.; Epstein, L. M. *J. Organomet. Chem.* **2002**, *657*, 155−162.
(63) Sivaev, I. B.; Bragin, V. I.; Prikaznov, A. V.; Petrovskii, P. V.; Bregadze, V. I.; Filippov, O. A.; Teplinskaya, T. A.; Titov, A. A.; Shubina, E. S. *Collect. Czech. Chem. Commun.* **2007**, *72*, 1725−1739.
(64) Bakhmutov, V. I. *Dihydrogen Bonds: Principles, Experiments, and Applications*; John Wiley & Sons, Inc.: Hoboken, NJ, 2008; p 241.
(65) Bakhmutov, V. I.; Bakhmutova, E. V.; Belkova, N. V.; Bianchini, C.; Epstein, L. M.; Masi, D.; Peruzzini, M.; Shubina, E. S.; Vorontsov, E. V.; Zanobini, F. *Can. J. Chem.* **2001**, *79*, 479−489.
(66) Güizado-Rodríguez, M.; Flores-Parra, A.; Sánchez-Ruiz, S. A.; Tapia-Benavides, R.; Contreras, R.; Bakhmutov, V. I. *Inorg. Chem.* **2001**, *40*, 3243−3246.
(67) Grabowski, S. J.; Sokalski, W. A.; Leszczynski, J. *J. Phys. Chem. A* **2005**, *109*, 4331−4341.
(68) Weinhold, F.; Klein, R. A. *Mol. Phys.* **2012**, *110*, 565−579.
(69) Filippov, O. A.; Belkova, N. V.; Epstein, L. M.; Lledós, A.; Shubina, E. S. *ChemPhysChem* **2012**, *13*, 2677−2687.
(70) Maseras, F.; Koga, N.; Morokuma, K. *Organometallics* **1994**, *13*, 4008−4016.
(71) Demachy, I.; Esteruelas, M. A.; Jean, Y.; Lledós, A.; Maseras, F.; Oro, L. A.; Valero, C.; Volatron, F. *J. Am. Chem. Soc.* **1996**, *118*, 8388−8394.
(72) Sabo-Etienne, S.; Chaudret, B. *Chem. Rev.* **1998**, *98*, 2077−2092.
(73) Kubas, G. J. The Extraordinary Dynamic Behavior and Reactivity of Dihydrogen and Hydride in the Coordination Sphere of Transition Metals. In *Hydrogen-Transfer Reactions*; Wiley-VCH Verlag GmbH & Co. KGaA: Hoboken, NJ, 2007; pp 603−637.
(74) Sandoval, C. A.; Ohkuma, T.; Muñiz, K.; Noyori, R. *J. Am. Chem. Soc.* **2003**, *125*, 13490−13503.
(75) Sandoval, C. A.; Yamaguchi, Y.; Ohkuma, T.; Kato, K.; Noyori, R. *Magn. Reson. Chem.* **2006**, *44*, 66−75.